An International Journal of Optimization and Control: Theories & Applications
ISSN: 2146-0957 eISSN: 2146-5703
Vol.15, No.3, pp.517-534 (2025)
https://doi.org/10.36922/IJOCTA025080034

RESEARCH ARTICLE

Proportional integral derivative plus control for nonlinear discrete-time state-dependent parameter: Industrial applications

E. M. Shaban[1,2*]

[1]Department of Mechanical Engineering Technology, College of Applied Industrial Technology, Jazan University, Jazan, Saudi Arabia
[2]On leave from Faculty of Engineering (Mataria), Helwan University, Cairo, Egypt
eeshaban@jazanu.edu.sa

ARTICLE INFO

Article History:
Received: February 21, 2025
1st revised: March 2, 2025
2nd revised: March 20 , 2025
Accepted: April 11, 2025
Published Online: July 16, 2025

Keywords:
Proportional-integral-derivative control
State-dependent parameter models
Non-minimal state space
State variable feedback

AMS Classification:
37H05, 37M05, 37M10, 37M15, 37N35, 37N40, 65P40, 70Q05, 70K70

ABSTRACT

In modern industrial automation, control of nonlinear systems with complex dynamics poses significant challenges, especially when dealing with discrete-time models that incorporate state-dependent parameters. Addressing this need, this paper explores the Proportional-integral-derivative-plus (PID+) control approach applied to nonlinear systems characterized by state-dependent parameter (SDP) discrete-time models. Two industrial applications are demonstrated as follows: a bitumen tank system and a reeling/packing machine used in a bitumen membrane sheet production line. Both systems are modeled using discrete-time transfer functions with SDP structures. The present work extends the novel SDP-PID+ approach by formulating its control algorithms and integrating additional proportional and input compensators. This enhancement enables effective and intuitive handling of processes characterized by discrete-time transfer functions with any order and sampling time delay. The approach enables a straightforward implementation of the SDP-PID+ algorithm across two distinct industrial applications, considering their varying response times. The approach reduces the time required to design the SDP-PID+ method for the selected applications while also demonstrating enhanced robustness and performance. It effectively mitigates disturbances and accommodates nonlinearities, higher-order dynamics, and delays.

1. Introduction

Proportional integral derivative (PID) controllers have been widely used in industrial processes since their development in the mid-1950s.[1,2] Today, they remain the most prevalent method for controlling process variables due to their simplicity and reliability.[3] Research has continually refined PID tuning methods, introducing approaches such as auto-tuning,[4,5] genetic tuning,[5,6] robust tuning,[7] and optimal tuning.[8] However, significant challenges arise when addressing processes with high-order transfer functions (TFs), $n \geq 3$, time delays greater than unity, $\delta \geq 2$, or nonlinearities.[9] The proportional integral derivative plus (PID+) control approach was developed to address these challenges as an extension of conventional PID methods. It integrates additional dynamic feedback and input compensators to handle processes with higher-order dynamics or pure time delays exceeding unity.[10] Unlike traditional PID control, PID+ employs state variable feedback (SVF) techniques, replacing manual tuning with pole assignment or linear quadratic (LQ) optimization strategies.[11] These enhancements improve control performance in systems that conventional PID tuning often struggles to manage effectively.[10,12]

*Corresponding Author

Previous research on PID+ controllers has demonstrated their applicability across many practical systems. Notable applications include robot arm control,[11,12] industrial temperature regulation of bitumen tank systems,[13] liquid storage tank loading/unloading control,[14] and speed control in reeling/packing machines equipped with field programmable gate array (FPGA) modules.[15] These applications cover systems with varying response times, from slow thermal processes to fast electric motors, and have shown consistent on-site success.

The theoretical foundation of PID+ control is built upon state-dependent parameter (SDP) models, which represent nonlinear systems using quasi-linear structures. These models describe system parameters as functions of state variables, allowing nonlinear dynamics to be approximated as linear systems at each sampling instant.[16] Such SDP-TF models facilitate the design of nonlinear control laws using well-established linear techniques.[17–21] Additionally, incorporating non-minimal state space (NMSS) representations enables direct SVF control without observers or reconstructors, simplifying implementation.[22,23]

Conventional PID designs often fail to provide robust performance for high-order processes with significant delays. For example, Chien–Hrones–Reswick and Ziegler–Nichols tuning have produced noisy control actions in systems such as bitumen temperature regulation.[10] To address these limitations, the novel SDP-PID+ control strategy was introduced and applied in previous studies,[11,13–15] incorporating additional input/output compensators to address sampling delays and higher-order dynamics. Building upon this foundation, the present work further enhances the approach by formulating its control algorithms to regulate processes characterized by discrete-time TFs of any order effectively and with arbitrary sampling time delays. This refinement facilitates the seamless implementation of the SDP-PID+ algorithm across two distinct industrial applications,[13,15] in regards to their varying response times. Additionally, the approach streamlines the design process, reducing computational effort while enhancing robustness and closed-loop control performance. The two practical applications are as follows:

(i) Industrial bitumen tank system. Temperature regulation to ensure product quality and safety during mixing.[13]
(ii) Industrial reeling/packing machine. Speed control of a pulling motor on the bitumen membrane sheet production line using FPGA technology.[15]

The first demonstrator introduces a slow thermal dynamic system, focusing on temperature control of bitumen within a tank before it is mixed with additives such as polymers and fillers.[13] In contrast, the second demonstrator represents a fast response dynamic of an electric motor, specifically the speed control of the pulling motor in the reeling/packing machine used in the production line of bitumen membrane sheets.[15] FPGAs are leveraged to optimize performance in this application, taking advantage of their inherent parallel processing capabilities.[15]

Sections 2 and 3 outline the identification methodology and the extension of the SDP-PID+ approach, which facilitates the intuitive handling of processes characterized by discrete-time TFs of any order and sampling time delays. Sections 4 and 5 describe the seamless implementation of the approach for each demonstrator. Finally, conclusions are presented in Section 6.

2. System identification

2.1. Model structure

The deterministic form of the SDP-TF for single-input, single-output (SISO) models may be defined as[16,23] in Equation (1),

$$y_k = \Pi^T \Phi_k \tag{1}$$

where Π is a vector of lagged input and output variables and Φ_k is a vector of SDP parameters, defined in Equation (2).

$$\begin{aligned} \Pi^T &= \begin{bmatrix} -y_{k-1} & \dots & -y_{k-n} & u_{k-1} & \dots & u_{k-m} \end{bmatrix} \\ \Phi_k &= \begin{bmatrix} a_1\{\chi_k\} & \dots & a_n\{\chi_k\} & b_1\{\chi_k\} & \dots & b_m\{\chi_k\} \end{bmatrix}^T \end{aligned} \tag{2}$$

Here, y_k and u_k represent the system's output and control input, respectively, while $a_i\{\chi_k\}$ for $i = 1, \dots, n$ and $b_j\{\chi_k\}$ for $j = 1, \dots, m$ are SDPs for which they are assumed to be functions of a non-minimal state vector, χ_k, not necessarily y_{k-i}. or u_{k-j}. However, for the SDP-PID+ control system design in the current paper, it is sufficient to limit the model in Equation (1) to $\chi_k = \Pi$. It is worth noting that any time delay, i.e. $\delta \geq 1$, is accounted for by setting the leading terms $b_1\{\chi_k\} \dots b_{\delta-1}\{\chi_k\}$ to zero. Finally, n and m are integers representing the maximum lag associated with the output and input variables, respectively. Therefore, the SDP-TF in

Equation (1) may be expressed in discrete form as in Equation (3).

$$y_k = -\sum_{i=1}^{n} a_i\{\chi_k\}\, y_{k-i} + \sum_{j=1}^{m} b_{j+\delta-1}\{\chi_k\}\, u_{k-(j+\delta-1)} \tag{3}$$

The incremental form in Equation (3) can be expressed in a discrete-time SDP-TF representation using the backward shift operator z^{-1} as follows in Equation (4).

$$y_k = \frac{\sum_{j=1}^{m} b_{j+\delta-1}\{\chi_k\}\,\mathrm{z}^{-(j+\delta-1)}}{1+\sum_{i=1}^{n} a_i\{\chi_k\}\,\mathrm{z}^{-i}} u_k = \frac{B\left(\chi_k,\mathrm{z}^{-1}\right)}{A(\chi_k,\mathrm{z}^{-1})} u_k \tag{4}$$

Here, the output parameters, $a_1\{\chi_k\}, \ldots, a_n\{\chi_k\}$, determine the order of the SDP-TF in Equation (4), denoted as n, while the number of input parameters, $b_\delta\{\chi_k\}, \ldots, b_{m+\delta-1}\{\chi_k\}$, is denoted as m. The polynomials $A\left(\chi_k,\mathrm{z}^{-1}\right)$ and $B\left(\chi_k,\mathrm{z}^{-1}\right)$ represent the output and input parameters, respectively, using the backward shift operator z^{-i}, where n and $m+\delta-1$ are the orders of these polynomials.

Numerous recent publications have outlined an approach for identifying and estimating the SDP-TF in Equation (3) and its application to a wide range of dynamic systems.[10–17,23] This approach typically consists of model identification and parameter estimation, as discussed below.

2.2. Model identification

The model structure and its potential state variables are initially identified through statistical estimation of discrete-time linear TF models. These models follow a similar structure to Equation (1), with time-invariant parameters, i.e., a_i ($i = 1, \ldots, n$), and b_j ($j = 1, \ldots, m$) are constant coefficients. These coefficients are estimated using the simplified refined instrumental variable algorithm. The appropriate linear model structure, i.e., triad $\{n, m, \delta\}$, is determined based on two statistical measures: (i) the coefficient of determination R_T^2, which evaluates the fit based on the response error, and (ii) Young's identification criterion, a hybrid measure that combines model fit and parametric efficiency.[24–29]

Following linear model identification, stochastic time-varying parameter models are estimated using recursive Kalman filtering and fixed interval smoothing algorithms.[23] These methods capture parameter variations driven by state variables or other dynamics, enabling nonlinear or chaotic behavior modeling. The recursive Kalman filtering/fixed interval smoothing approach employs iterative "back fitting" with reordered time-series data to refine the parameter estimates in Equation (1). The approach exists in MATLAB® as a computer-aided program for time series analysis and identification of noisy systems toolbox.[24–32]

2.3. Parameter estimation

Each element of Φ_k in the SDP-TF model in Equation (1) represents a nonparametric estimate, varying at every sampling instant and visualized as a graph. To achieve a more compact representation, these nonlinearities can be parameterized in terms of their associated dependent variable[23] using functions or neural networks and optimized via deterministic least squares or statistically efficient methods. However, for the applications considered here, linear functions of the state variables suffice for control design.[16]

3. Control methodology

3.1. State-dependent parameter-proportional-integral-derivative-plus control

The typical structure of a discrete PID controller is illustrated in Figure 1. It employs three compensators as follows: proportional ($k_{P1,k}$), integral ($k_{I,k}$), and derivative ($k_{D,k}$), of which all act on the error signal $e_k = r_k - y_k$, where r_k is the reference signal, and y_k is the system output. This structure provides an SVF formulation for PID control (SVF/PID) as in Equation (5).

$$\begin{aligned} u_k &= k_{I,k}\,\frac{e_k}{1-\mathrm{z}^{-1}} + k_{P1,k}\,e_k + k_{D,k}\left(1-\mathrm{z}^{-1}\right)e_k \\ &= \begin{bmatrix} k_{I,k} & k_{P1,k} & k_{D,k} \end{bmatrix} \begin{bmatrix} z_k \\ e_k \\ \Delta e_k \end{bmatrix} \end{aligned} \tag{5}$$

Here, $\begin{bmatrix} z_k & e_k & \Delta e_k \end{bmatrix}^T$ is the feedback state vector, given that e_k is the error state, Δe_k is the difference of error state and $z_k = z_{k-1} + e_k$ is the integral of the error state. The SDP-TF model in Equation (4) within the PID control methodology, as depicted in Figure 1, typically results in state-dependent compensators that justify the term SDP-PID control. The subscript k in the elements of the control vector $\begin{bmatrix} k_{I,k} & k_{P1,k} & k_{D,k} \end{bmatrix}$ in Equation (5) indicates the time-varying state feedback compensators, which are inherently state-dependent.

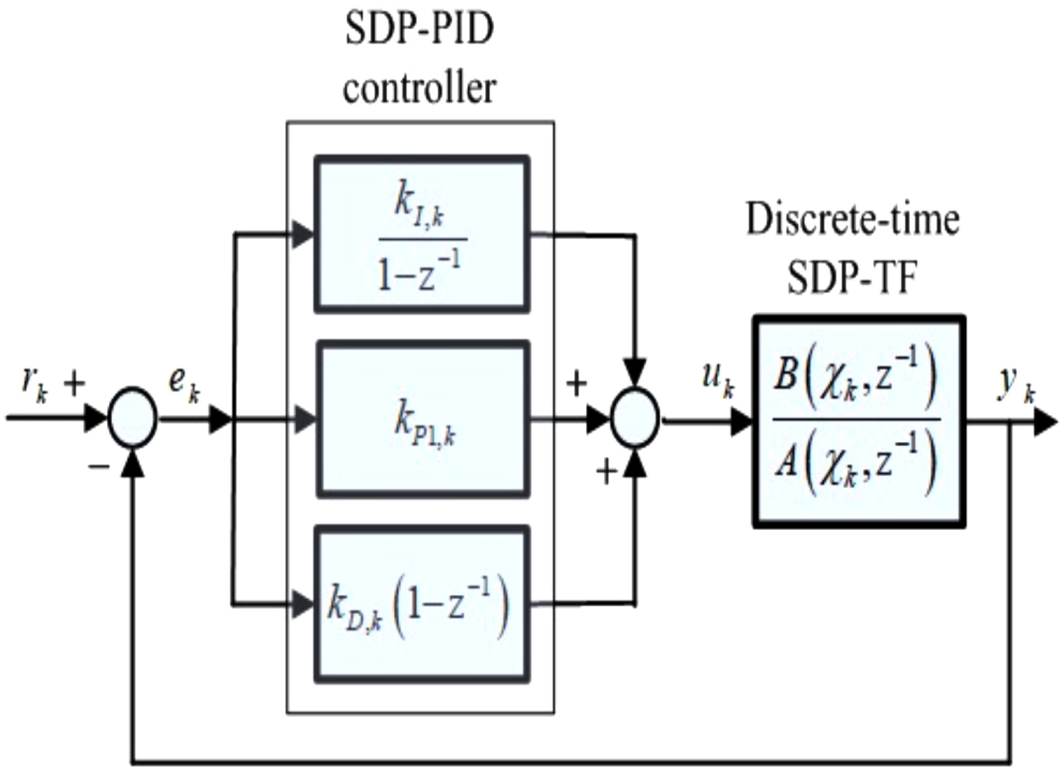

Figure 1. Typical structure of the discrete SDP-PID controller
Abbreviations: PID, proportional integral derivative; SDP, state-dependent parameter; TF, transfer function.

The PID structure, shown in Figure 1, is best suited for systems with discrete time SDP-TF of at most second order ($n \leq 2$), and unity sample time delays ($\delta = 1$). To extend its applicability, the regulator structure is employed, where the reference signal is set to zero, i.e. $r_k = 0$, making the error signal $e_k = -y_k$, and treating external disturbances as changes in the reference signal, r_k, [11–15,17] as depicted in Figure 2. This is possible because the external set point does not affect the control process .[33,34] This regulator form modifies Equation (4) to the following form in Equation (6).

$$e_k = \frac{-\sum_{j=1}^{m} b_{j+\delta-1}\{\chi_k\}\, z^{-(j+\delta-1)}}{1+\sum_{i=1}^{n} a_i\{\chi_k\}\, z^{-i}} u_k = \frac{-B\left(\chi_k, z^{-1}\right)}{A\left(\chi_k, z^{-1}\right)} u_k \tag{6}$$

To accommodate higher-order processes ($n > 2$) and numerator polynomials of order greater than unity ($m + \delta - 1 > 1$), the SDP-PID+ approach introduces additional compensators, called *plus* gains, that decelerate control actions and enhance stability. These innovative *plus* gains mirror the term SDP-PID+. Given the regulator SDP-PID+ structure, as depicted in Figure 2, the NMSS representation for SDP-PID+ control is given in Equation (7).

$$\begin{aligned} \mathbf{x}_k &= \mathbf{F}_k\, \mathbf{x}_{k-1} + \mathbf{g}_k\, u_{k-1} \\ y_k &= \mathbf{h}\, \mathbf{x}_k \end{aligned} \tag{7}$$

Equation (7) enables the direct implementation of full SVF control using the measured input and output signals of the controlled system without requiring the design of a state reconstructor.[16] Here, the k^{th} sample of the non-minimal feedback state vector is defined in Equation (8).

$$\mathbf{x}_k = \left[\begin{array}{c} \underbrace{z_k \quad e_k \quad \Delta e_k}_{\substack{\text{Typical PID feedback states} \\ n \leq 2}} \\ \underbrace{e_{k-2} \quad e_{k-3} \quad \cdots \quad e_{k-(n-2)} \quad e_{k-(n-1)}}_{\substack{\text{Extra proportional feedback states if} \\ n>2}} \\ \underbrace{u_{k-1} \quad u_{k-2} \quad \cdots \quad u_{k-(m+\delta-3)} \quad u_{k-(m+\delta-2)}}_{\substack{\text{Extra input feedback states} \\ \text{if } m \geq 1 \text{ and/or } \delta>1}} \end{array}\right]^T \tag{8}$$

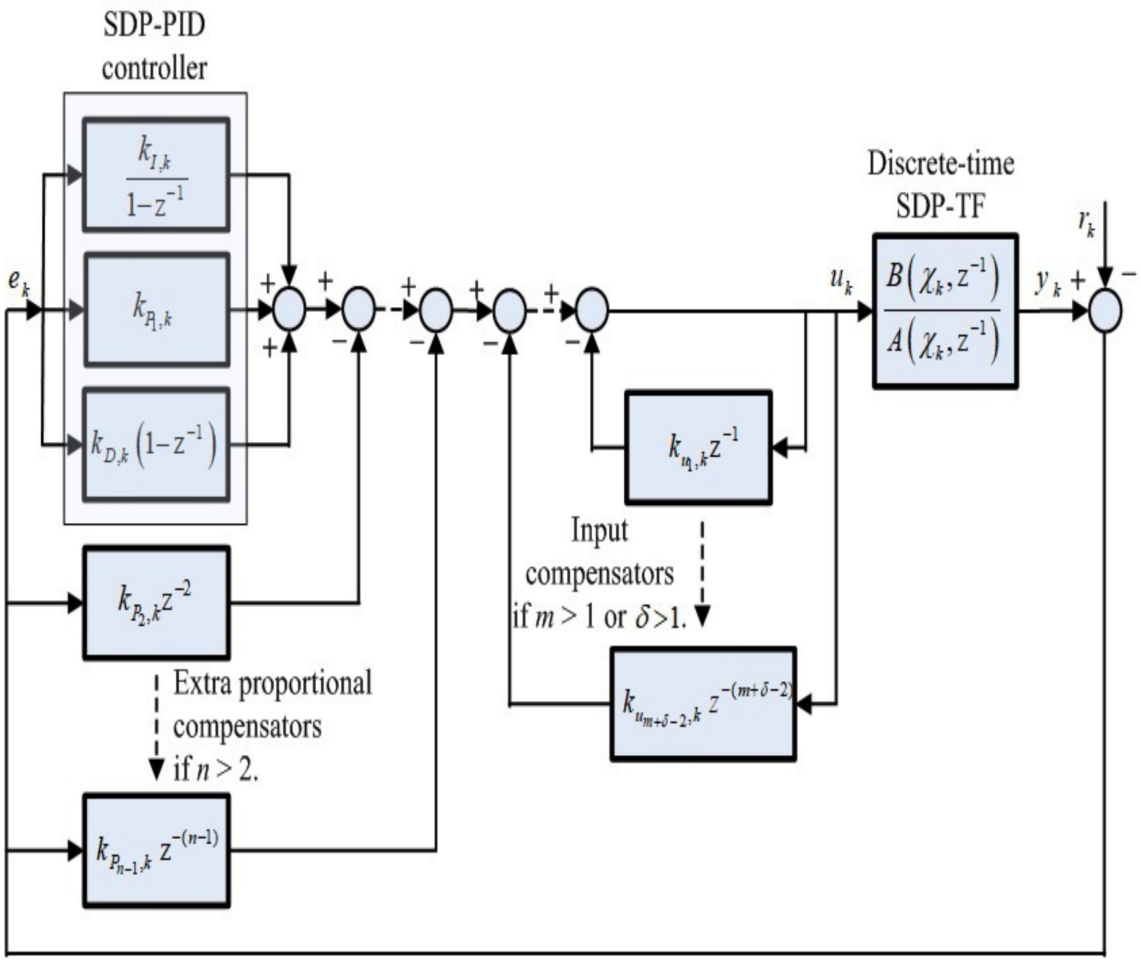

Figure 2. Regulator structure of the discrete SDP-PID+ controller, where the reference signal, r_k, is treated as a disturbance applied to the control system. Abbreviations: PID, proportional integral derivative; SDP, state-dependent parameter; TF, transfer function

The integral of error state, $z_k = z_{k-1} + e_k$, is exploited for NMSS design to introduce the inherent type 1 servomechanism performance .[35]

Given the SDP-TF model in Equation (6), the error state depicted in Equation (8), e_k, can be evaluated as in Equation (9).

$$\begin{aligned} e_k = -y_k = &-(a_{1,k} + a_{2,k})\, e_{k-1} + a_{2,k}\, \Delta e_{k-1} \\ &- a_{3,k}\, e_{k-3} - \ldots - a_{n-1,k}\, e_{k-(n-1)} \\ &- a_{n,k}\, e_{k-n} \\ &- b_{1,k}\, u_{k-1} - \ldots - b_{m-1,k}\, u_{k-(m-1)} \\ &- b_{m,k}\, u_{k-m} \end{aligned} \tag{9}$$

For the sake of generalization, the time delay in Equation (9) is assumed to be unity ($\delta = 1$), and the SDP-TF in Equation (4) is considered with at least second order ($n \geq 2$). Additionally, the terms $a_i\{\chi_k\}$ and $b_j\{\chi_k\}$ have been replaced by $a_{i,k}$ ($\forall\ i = 1, \ldots, n$) and $b_{j,k}$ ($\forall\ j = 1, \ldots, m$) respectively, for brevity. The integral of the error state, z_k, and the difference in the error state, Δe_k, can be evaluated from Equation (9) as follows in Equations (10) and (11).

$$\begin{aligned} z_k = z_{k-1} &- (a_{1,k} + a_{2,k})\, e_{k-1} + a_{2,k}\, \Delta e_{k-1} \\ &- a_{3,k}\, e_{k-3} - \ldots - a_{n-1,k}\, e_{k-(n-1)} - a_{n,k}\, e_{k-n} \\ &- b_{1,k}\, u_{k-1} - \ldots - b_{m-1,k}\, u_{k-(m-1)} - b_{m,k}\, u_{k-m} \end{aligned} \tag{10}$$

$$\begin{aligned} \Delta e_k = &-(a_{1,k} + a_{2,k} + 1)\, e_{k-1} + a_{2,k}\, \Delta e_{k-1} \\ &- a_{3,k}\, e_{k-3} - \ldots - a_{n-1,k}\, e_{k-(n-1)} - a_{n,k}\, e_{k-n} \\ &- b_{1,k}\, u_{k-1} - \ldots - b_{m-1,k}\, u_{k-(m-1)} - b_{m,k}\, u_{k-m} \end{aligned} \tag{11}$$

The set of Equations (9-11) can be used to derive the NMSS/SDP-PID+ form in Equation (7), considering the state feedback vector defined in Equation (8). The general form of the state transition square matrix $\mathbf{F}_k$ of order $n + m + \delta - 1$ ($\forall\ n \geq 2$), the input vector $\mathbf{g}_k$, and the time-invariant observation vector $\mathbf{h}$, at the k^{th} sample, are defined as follows in Equation (12).

$$\mathbf{F}_k = \begin{bmatrix} \underbrace{\mathbf{F}_{1,k}}_{(n+m+\delta-1)\times 3} & \underbrace{\mathbf{F}_{2,k}}_{(n+m+\delta-1)\times(n-2)} & \underbrace{\mathbf{F}_{3,k}}_{(n+m+\delta-1)\times(m+\delta-2)} \end{bmatrix}_{(n+m+\delta-1)\times(n+m+\delta-1)} \tag{13}$$

$$\mathbf{g}_k = \begin{bmatrix} \underbrace{-b_{1,k} \quad -b_{1,k} \quad -b_{1,k}}_{3} & \underbrace{0 \quad 0 \quad \dots \quad 0 \quad 0}_{n-2} & \underbrace{1 \quad 0 \quad \dots \quad 0 \quad 0}_{m+\delta-2} \end{bmatrix}^T \tag{12}$$

$$\mathbf{h} = \begin{bmatrix} \underbrace{0 \quad -1 \quad 0}_{3} & \underbrace{0 \quad 0 \quad \dots \quad 0 \quad 0}_{n-2} & \underbrace{0 \quad 0 \quad \dots \quad 0 \quad 0}_{m+\delta-2} \end{bmatrix}$$

The submatrices $\mathbf{F}_{1,k}$, $\mathbf{F}_{2,k}$, and $\mathbf{F}_{3,k}$ are defined as follows in Equation (13).

$$\mathbf{F}_{1,k} = \begin{bmatrix} 1 & 0 & 0 & 0 & 0 & \dots & 0 & 0 & 0 & 0 & \dots & 0 & 0 \\ -(a_{1,k}+a_{2,k}) & -(a_{1,k}+a_{2,k}) & -(a_{1,k}+a_{2,k}+1) & 0 & 0 & \dots & 0 & 0 & 0 & 0 & \dots & 0 & 0 \\ a_{2,k} & a_{2,k} & a_{2,k} & 0 & 0 & \dots & 0 & 0 & 0 & 0 & \dots & 0 & 0 \end{bmatrix}^T \quad \leftrightarrow n = 2$$

$$\mathbf{F}_{2,k} = \begin{bmatrix} -a_{3,k} & -a_{3,k} & -a_{3,k} & 0 & 1 & \dots & 0 & 0 & 0 & 0 & \dots & 0 & 0 \\ -a_{4,k} & -a_{4,k} & -a_{4,k} & 0 & 0 & \ddots & 0 & 0 & 0 & 0 & \dots & 0 & 0 \\ \vdots & \vdots & \vdots & \vdots & \vdots & \vdots & \ddots & \vdots & \vdots & \vdots & \dots & \vdots & \vdots \\ -a_{n-2,k} & -a_{n-2,k} & -a_{n-2,k} & 0 & 0 & \dots & 0 & 1 & 0 & 0 & \dots & 0 & 0 \\ -a_{n-1,k} & -a_{n-1,k} & -a_{n-1,k} & 0 & 0 & \dots & 0 & 0 & 0 & 0 & \dots & 0 & 0 \end{bmatrix}^T \quad \leftrightarrow n > 2$$

$$\mathbf{F}_{3,k} = \begin{bmatrix} -b_{2,k} & -b_{2,k} & -b_{2,k} & 0 & 0 & \dots & 0 & 0 & 0 & 1 & \dots & 0 & 0 \\ -b_{3,k} & -b_{3,k} & -b_{3,k} & 0 & 0 & \dots & 0 & 0 & 0 & 0 & \ddots & 0 & 0 \\ \vdots & \vdots & \vdots & \vdots & \vdots & \dots & \vdots & \vdots & \vdots & \vdots & \dots & \ddots & \vdots \\ -b_{m+\delta-2,k} & -b_{m+\delta-2,k} & -b_{m+\delta-2,k} & 0 & 0 & \dots & 0 & 0 & 0 & 0 & \dots & 0 & 1 \\ -b_{m+\delta-1,k} & -b_{m+\delta-1,k} & -b_{m+\delta-1,k} & 0 & 0 & \dots & 0 & 0 & 0 & 0 & \dots & 0 & 0 \end{bmatrix}^T \quad \leftrightarrow m+\delta > 2 \tag{13}$$

As depicted in Equation (13), the submatrices $\mathbf{F}_{2,k}$ and $\mathbf{F}_{3,k}$ exist if and only if $n > 2$ and $m + \delta > 2$, respectively. Therefore, in case of $n = 2$ and $m + \delta = 2$, there is no plus, and the definition in Equation (12) is downgraded to the NMSS/SDP-PID form as follows in Equation (14).

$$\begin{aligned} \mathbf{F}_k &= \begin{bmatrix} 1 & -(a_{1,k}+a_{2,k}) & a_{2,k} \\ 0 & -(a_{1,k}+a_{2,k}) & a_{2,k} \\ 0 & -(a_{1,k}+a_{2,k}+1) & a_{2,k} \end{bmatrix}, \\ \mathbf{g}_k &= \begin{bmatrix} -b_{1,k} \\ -b_{1,k} \\ -b_{1,k} \end{bmatrix}, \\ \textit{and } \mathbf{h} &= \begin{bmatrix} 0 & -1 & 0 \end{bmatrix} \end{aligned} \tag{14}$$

Here, the state feedback vector is as presented in Equation (15),

$$\mathbf{x}_k = \begin{bmatrix} z_k & e_k & \Delta e_k \end{bmatrix}^T \tag{15}$$

for which the states are given as in Equation (16).

$$\begin{aligned} e_k &= -(a_{1,k}+a_{2,k})\, e_{k-1} + a_{2,k}\, \Delta e_{k-1} - b_{1,k}\, u_{k-1} \\ z_k &= z_{k-1} - (a_{1,k}+a_{2,k})\, e_{k-1} + a_{2,k}\, \Delta e_{k-1} - b_{1,k}\, u_{k-1} \\ \Delta e_k &= -(a_{1,k}+a_{2,k}+1)\, e_{k-1} + a_{2,k}\, \Delta e_{k-1} - b_{1,k}\, u_{k-1} \end{aligned} \tag{16}$$

Also, in the case of the discrete-time SDP-TF model with unity order, i.e. $n = 1$, and $m+\delta > 2$, the submatrix $\mathbf{F}_{2,k}$ vanishes, and the third column in the submatrix $\mathbf{F}_{1,k}$ becomes zero-valued. Consequently, this results in the NMSS/SDP-PI+ representation without a *derivative* component, as the third column vector of the submatrix $\mathbf{F}_{1,k}$, associated with the derivative state, Δe_{k-1}, is zero.[17] Under this condition, the states defined in Equations (9-11) are reduced to Equation (17).

$$\begin{aligned} e_k =& -a_{1,k}\, e_{k-1} - b_{1,k}\, u_{k-1} - \dots \\ & - b_{m-1,k}\, u_{k-(m-1)} - b_{m,k}\, u_{k-m} \\ z_k =& z_{k-1} - a_{1,k}\, e_{k-1} - b_{1,k}\, u_{k-1} - \dots \\ & - b_{m-1,k}\, u_{k-(m-1)} - b_{m,k}\, u_{k-m} \end{aligned} \tag{17}$$

Thus, for $n = 1$ and $m + \delta > 2$, the set of Equation (17) represents the NMSS/SDP-PI+ form using the following state feedback vector in Equation (18).

$$\mathbf{x}_k = \begin{bmatrix} z_k & e_k & u_{k-1} & u_{k-2} & \dots, \\ u_{k-(m+\delta-3)} & u_{k-(m+\delta-2)} \end{bmatrix}^T \tag{18}$$

The state transition square matrix $\mathbf{F}_k$ (order $m + \delta$), the input vector $\mathbf{g}_k$, and the observation vector $\mathbf{h}$ are now defined as Equation (19).

$$\mathbf{F}_k = \begin{bmatrix} 1 & -a_{1,k} & -b_{2,k} & -b_{3,k} & \dots & -b_{m+\delta-2,k} & -b_{m+\delta-1,k} \\ 0 & -a_{1,k} & -b_{2,k} & -b_{3,k} & \dots & -b_{m+\delta-2,k} & -b_{m+\delta-1,k} \\ 0 & 0 & 0 & 0 & \dots & 0 & 0 \\ 0 & 0 & 1 & 0 & \dots & 0 & 0 \\ \vdots & \vdots & \vdots & \ddots & \vdots & \vdots & \vdots \\ 0 & 0 & 0 & 0 & \ddots & 0 & 0 \\ 0 & 0 & 0 & 0 & 0 & 1 & 0 \end{bmatrix}$$

$$\leftrightarrow \begin{cases} n = 1 \\ m + \delta > 2 \end{cases}$$

$$\mathbf{g}_k = \begin{bmatrix} -b_{1,k} & -b_{1,k} & 1 & 0 & \dots & 0 & 0 \end{bmatrix}^T$$

$$\mathbf{h} = \begin{bmatrix} 0 & -1 & 0 & 0 & \dots & 0 & 0 \end{bmatrix} \tag{19}$$

It is always possible to derive the NMSS/SDP-PID+ for the discrete-time SDP-TF model with the first order, $n = 1$, and $m + \delta > 2$. This is achieved by assuming that, as the controlled process approaches a steady state, i.e. $e_k \to 0$, the second difference of the error state also tends to zero, i.e., $\Delta^2 e_k \to 0$. Consequently, the first difference of the error state can be considered constant, i.e., $\Delta e_k \cong c$.[13] In this case, the states in Equation (17) may be rewritten as Equation (20).

$$\begin{aligned} e_k &= -a_{1,k}\, e_{k-1} - b_{1,k}\, u_{k-1} - \dots \\ &\quad - b_{m-1,k}\, u_{k-(m-1)} - b_{m,k}\, u_{k-m} \\ z_k &= z_{k-1} - a_{1,k}\, e_{k-1} - b_{1,k}\, u_{k-1} - \dots \\ &\quad - b_{m-1,k}\, u_{k-(m-1)} - b_{m,k}\, u_{k-m} \\ \Delta e_k &= \frac{\Delta e_k + \Delta e_{k-1}}{2} \\ &\quad - (a_{1,k} + 1)\; e_{k-1} - b_{1,k}\, u_{k-1} - \dots \\ &= \frac{-b_{m-1,k}\, u_{k-(m-1)} - b_{m,k}\, u_{k-m} + \Delta e_{k-1}}{2} \end{aligned} \tag{20}$$

The state definition in Equation (20) restores the NMSS/SDP-PID+ form for the first-order SDP-TF model using the following state feedback vector in Equation (21).

$$\mathbf{x}_k = \begin{bmatrix} z_k\; e_k \Delta e_k\; u_{k-1}\; u_{k-2}\; ..., \\ u_{k-(m+\delta-3)}\; u_{k-(m+\delta-2)} \end{bmatrix}^T \tag{21}$$

The square matrix $\mathbf{F}_k$ of order $m + \delta + 1$ ($\forall\; n = 1$), the input vector $\mathbf{g}_k$, and the observation vector $\mathbf{h}$ are defined as Equation(22).

$$\mathbf{F}_k = \begin{bmatrix} 1 & -a_{1,k} & 0 & -b_{2,k} & -b_{3,k} & \dots & -b_{m+\delta-2,k} & -b_{m+\delta-1,k} \\ 0 & -a_{1,k} & 0 & -b_{2,k} & -b_{3,k} & \dots & -b_{m+\delta-2,k} & -b_{m+\delta-1,k} \\ 0 & \frac{-a_{1,k}}{2} & \frac{1}{2} & \frac{-b_{2,k}}{2} & \frac{-b_{3,k}}{2} & \dots & \frac{-b_{m+\delta-2,k}}{2} & \frac{-b_{m+\delta-1,k}}{2} \\ 0 & 0 & 0 & 0 & 0 & \dots & 0 & 0 \\ 0 & 0 & 0 & 1 & 0 & \dots & 0 & 0 \\ \vdots & \vdots & \vdots & \vdots & \ddots & \dots & \vdots & \vdots \\ 0 & 0 & 0 & 0 & 0 & \ddots & 0 & 0 \\ 0 & 0 & 0 & 0 & 0 & \dots & 1 & 0 \end{bmatrix}$$

$$\leftrightarrow \begin{cases} n = 1 \\ m + \delta > 2 \end{cases}$$

$$\mathbf{g}_k = \begin{bmatrix} \frac{-b_{1,k}}{2} & \frac{-b_{1,k}}{2} & \frac{-b_{1,k}}{2} & 1 & 0 & \dots & 0 & 0 \end{bmatrix}^T$$

$$\mathbf{h} = \begin{bmatrix} 0 & -1 & 0 & 0 & 0 & \dots & 0 & 0 \end{bmatrix} \tag{22}$$

The methodology for deriving the SDP-PID+ and its variants is summarized in Table 1 for clarity and to disentangle the equations.

3.2. Controllability

The linear-like structure of the SDP-TF model in Equation (4) facilitates the design of the nonlinear SDP-PID+ control law using the strategies of the linear system design, such as suboptimal LQ or pole assignment approaches.[10–15] However, using these basic methods, some SDP-TF model structures may not be fully controllable.[38]

In control theory, controllability refers to the ability to drive a system's state to any desired state within a finite time, starting from any initial condition. For the SDP-TF model in Equation (4), discrete controllability at each sample k means the system can be controlled at each sampling instance. This, necessarily, leads to a system $\mathbf{F}_k$, $\mathbf{g}_k$, and $\mathbf{h}$ of NMSS/SDP-PID+, which is controllable over each sampling period.[38,39] The controllability conditions can be stated as:[39] Given a discrete-time SISO system described by Equation (4), the NMSS/SDP-PID+ form in Equation (7), characterized by the pair [$\mathbf{F}_k$ and $\mathbf{g}_k$], is locally controllable over each sampling period if and only if, the polynomials $A\left(\chi_k, \mathrm{z}^{-1}\right)$ and $B\left(\chi_k, \mathrm{z}^{-1}\right)$ are co-prime, and Equation (23) is met.

$$\sum_{j=1}^{m} b_{j+\delta-1}\left\{\chi_k\right\} \mathrm{z}^{-(j+\delta-1)} \neq 0 \tag{23}$$

Due to the time-varying nature of the parameters in the SDP case, it is important to note that these conditions may not always be met in every sample period. As a result, challenges may emerge during the control design process for the SDP-PID+ controller.

Although deriving comprehensive results for the controllability and stability of the nonlinear SDP system remains an area of ongoing research,[38,39] the practical approach described

Table 1. State-dependent parameters-proportional integral derivative plus methodology for the non-minimal state space representation in Equation (7)

Parameter	Control scheme	Description
$n \geq 2$ $m+\delta > 2$	This is the general SDP-PID+	• The state vector is defined in Equation (8) • The states are defined at Equations (9-11) • The matrices, $\mathbf{F}_k$, $\mathbf{g}_k$, and $\mathbf{h}$, of the order, $n+m+\delta-1$ are defined in Equations (12) and (13).
$n = 2$ $m+\delta = 2$	There are no plus gains SDP-PID+ switches to conventional SDP-PID	• The state vector is defined in Equation (15) • The states are defined in Equation (16) • The matrices, $\mathbf{F}_k$, $\mathbf{g}_k$, and $\mathbf{h}_k$, of the order $n+m+\delta-1$ are defined in Equation (14)
$n = 1$ $m+\delta > 2$	Special case: No derivative gain SDP-PID+ downgrades to SDP-PI+	• The state vector is defined in Equation (18) • The states are defined in Equation (17) • The matrices, $\mathbf{F}_k$, $\mathbf{g}_k$, and $\mathbf{h}$, of the order $m+\delta$ are defined in Equation (19)
$n = 1$ $m+\delta > 2$	Special case: Restoring derivative gain SDP-PI+ is upgraded back to SDP-PID+	• The state vector is defined in Equation (21) • The states are defined in Equation (20) • The matrices, $\mathbf{F}_k$, $\mathbf{g}_k$, and $\mathbf{F}_k$, of the order are $m+\delta+1$ defined in Equation (22)

Abbreviations: PI+: Proportional integral plus; PID: Proportional integral derivative; SDP: State-dependent parameter; TF: Transfer function.

above has been sufficient for the two demonstrators in this paper. This is because, in real-world applications, system variables are constrained and consistently remain within known boundaries.

3.3. Control algorithm

The SVF control is introduced in Equation (5) and can be expressed in its general form as follows in Equation (24).

$$u_k = -\mathbf{k}_k^+ \mathbf{x}_k \tag{24}$$

In Equation (24), the vector of the control gain, denoted as $\mathbf{k}_k$, is defined as

$$K_K{}^+ = \left[\begin{array}{c} \underbrace{k_{I,k} \quad k_{P_1,k} \quad k_{D,k},}_{\text{Typical PID gains, } n\leq 2} \\ \underbrace{k_{P_2,k} \quad k_{P_3,k} \quad \dots \quad k_{P_{n-2},k}, \quad k_{P_{n-1},k},}_{\text{Extra proportional gains, } n>2} \\ \underbrace{k_{u_1,k} \quad k_{u_2,k} \quad \dots \quad k_{u_{m+\delta-3},k}, \quad k_{u_{m+\delta-2},k}}_{\text{Extra input gains, } m+\delta\geq 2} \end{array}\right]^T \tag{25}$$

The SVF control vector in Equation (25) is computed at every sampling interval using either the pole placement technique or by minimizing an LQ cost function. In the latter method, the system is treated as a "frozen parameter" system, representing a specific instant of the family of the NMSS model [$\mathbf{F}_k$ and $\mathbf{g}_k$]. Alternatively, the discrete-time algebraic Riccatti equation is solved for each sampling interval.[33,36] For the pole placement approach, linear techniques are commonly employed to determine control gains, as demonstrated in .[11,12]

3.3.1. SDP-PID+/LQ tuning approach

The optimal SVF/SDP-PID+ control gain vector, as defined in Equation (25), can be determined by minimizing the following infinite-time optimal LQ cost function in Equation (26).

$$J = \sum_{k=0}^{\infty} \left[\mathbf{x}_k^T \, \mathbf{Q} \, \mathbf{x}_k + R \, u_k^2\right] \tag{26}$$

In Equation (26), R is a positive scalar that weights the input u_k and Q is a symmetric positive definite matrix that assigns weights to the states, as defined in Equation (8). For SISO systems, Q may be defined as in Equation (27).

$$\mathbf{Q} = \text{diag}\left\{\begin{array}{c} q_z \quad q_{e_1} \quad q_{\Delta e}, \\ q_{e_2} \; q_{e_3} \quad \cdots \quad q_{e_{n-2}} \quad q_{e_{n-1}}, \\ q_{u_1} \quad q_{u_2} \quad \cdots \quad q_{u_{m+\delta-3}} \quad q_{u_{m+\delta-2}} \end{array}\right\} \tag{27}$$

Based on the NMSS/SDP-PID+ form in Equation (7) with the description $\mathbf{F}_k$ and $\mathbf{g}_k$ as provided in Table 1, the time-varying SVF compensator vector, $\mathbf{k}_k^+$, of the nonlinear SDP-PID+ control, can be recursively determined as the steady state solution of the algebraic Riccati equation.[37] This equation is derived from the standard LQ cost function in Equation (26) at the k^{th} sample as follows in Equation (28),

$$\begin{aligned} \mathbf{k}_k^+ &= \left[\mathbf{g}_k^T \mathbf{P}^{(i+1)} \mathbf{g}_k + R\right]^{-1} \mathbf{g}_k^T \mathbf{P}^{(i+1)} \mathbf{F}_k \\ \mathbf{P}^{(i)} &= \mathbf{F}_k^T \mathbf{P}^{(i+1)} \left[\mathbf{F}_k - \mathbf{g}_k \, \mathbf{k}_k^+\right] + \mathbf{Q} \end{aligned} \tag{28}$$

where P is a symmetric positive definite matrix with the initial value $\mathbf{P}^{(i+1)} = \mathbf{Q}$ and $\mathbf{k}_k^+$ is the

SVF/SDP-PID+ control gain vector, as defined in Equation (25).

For simplicity, a frozen parameter system $\{\mathbf{F}'_k,\ \mathbf{g}'_k\}$ can be employed, where the frozen system is defined as a single sample instance from the family of $\{\mathbf{F}_k,\ \mathbf{g}_k\}$.[36,37] In this scenario, the matrix $\mathbf{P}$ becomes time-invariant, and Equation (28) is simplified to

$$\mathbf{P}^{(i)} = \mathbf{F'}_k^T \mathbf{P}^{(i+1)} \left[\mathbf{F'}_k - \mathbf{g}_k \left(\mathbf{g'}_k^T \mathbf{P}^{(i+1)} \mathbf{g'}_k + R\right)^{-1} \mathbf{g'}_k^T \mathbf{P}^{(i+1)} \mathbf{F'}_k\right] + \mathbf{Q} \tag{29}$$

After obtaining the matrix P from Equation (29), the SDP gain vector $\mathbf{k}_k^+$ can be derived from Equation (28) as follows:

$$\mathbf{k}_k^+ = \left[\mathbf{g}_k^T \mathbf{P}\ \mathbf{g}_k + R\right]^{-1} \mathbf{g}_k^T \mathbf{P}\ \mathbf{F}_k \tag{30}$$

Note that the system matrices $\{\mathbf{F}_k,\ \mathbf{g}_k\}$ remain unfrozen when implementing Equation (30). A straightforward trial and error approach is employed to evaluate the gain vector in Equation (30). The process begins with unity weights to ensure a balanced influence of each parameter, preventing any single parameter from dominating the others. This approach allows for consistent and logical experimentation.

3.3.2. SDP-PID+/pole placement tuning approach

The design methodology for discrete SDP-PID+/pole placement was introduced by Shaban et al.[11] It has been shown that the process is relatively straightforward, provided the performance of the closed-loop control system is predictable, i.e., if the SDP-TF in Equation (4) is controllable. Here, the nonlinear SDP-PID+ compensators, as defined in Equation (25), can be evaluated by modifying the location of the poles of the closed-loop SDP-PID+ control system. In this regard, the regulator structure of the SDP-PID+ controller, depicted in Figure 2, needs to be reduced to the unity feedback closed-loop SDP-PID+ control system in TF form, as illustrated in Figure 3 as follows in Equation (31),

$$y_k = \frac{K_k^+\left(\mathrm{z}^{-1}\right) B\left(\chi_k, \mathrm{z}^{-1}\right)}{\Delta\, K_{u,k}(\mathrm{z}^{-1})\, A(\chi_k, \mathrm{z}^{-1}) + K_k^+(\mathrm{z}^{-1})\, B(\chi_k, \mathrm{z}^{-1})}\, r_k \tag{31}$$

given that $\Delta = 1 - \mathrm{z}^{-1}$ represents the difference operator. The characteristic equation for the SDP-PID+ control system is extracted from Equation (31) as Equation (32).

$$\Delta\, K_{u,k}\left(\mathrm{z}^{-1}\right)\ A\left(\chi_k, \mathrm{z}^{-1}\right) + K_k^+\left(\mathrm{z}^{-1}\right)\ B\left(\chi_k, \mathrm{z}^{-1}\right) \tag{32}$$

This equation is used to determine the SDP-PID+ compensators, $\mathbf{k}_k^+$, in Equation (25). It is worth noting that the order of characteristic Equation (32) is $n + m + \delta - 1,\ \forall\ n \geq 2$, with a minimum order of three for a discrete-time SDP-TF of triad $\{\leq 2,\ 1,\ 1\}$. The polynomials corresponding to the proportional *plus* compensator, $K_k^+\left(\mathrm{z}^{-1}\right)$, and input *plus* compensator, $K_{u,k}\left(\mathrm{z}^{-1}\right)$, are defined as in Equation (33),

$$\begin{aligned} K_k^+\left(\mathrm{z}^{-1}\right) &= k_{1,k} - k_{2,k}\mathrm{z}^{-1} + k_{3,k}\mathrm{z}^{-2} + \sum_{i=4}^{n+1} k_{i,k}\, \mathrm{z}^{-(i-1)} \\ K_{u,k}\left(\mathrm{z}^{-1}\right) &= 1 + \sum_{j=1}^{m+\delta-2} k_{u_j,k}\mathrm{z}^{-j} \end{aligned} \tag{33}$$

where,

$$\begin{aligned} k_{1.k} &= k_{P_1,k} + k_{I,k} + k_{D,k} \\ k_{2.k} &= k_{P_1,k} + 2k_{D,k} \\ k_{3.k} &= k_{D,k} + k_{P_{i-1},k} \qquad i = 3 \text{ if } n \geq 3 \\ &\vdots \\ k_{i,k} &= -k_{P_{i-2},k} + k_{P_{i-1},k} \quad 4 \leq i \leq n+1 \end{aligned} \tag{34}$$

The *plus* compensators, $k_{P_{i-1}}$ $(i = 3, ...,\ n{+}1)$ for $n \geq 3$ and k_{u_j} $(j = 1,\ \ldots m + \delta - 2)$ for $m{+}\delta > 2$, in Equations (33) and (34) allow for exploiting additional poles to suit the discrete-time SDP-TF in Equation (4) that exceeds second-order dynamics, i.e. $n \geq 3$, and has time delay and/or numerator order greater than unity, i.e. $m + \delta > 2$. Applying polynomial algebra to the characteristic Equation (32) as Equation (35)

$$\begin{aligned} &\Delta\, K_{u,k}\left(z^{-1}\right) A_k\left(\chi_k, z^{-1}\right) + K_k^+\left(z^{-1}\right)\ B_k\left(\chi_k, z^{-1}\right) \\ =&(1 - p_1\, \mathrm{z}^{-1})\,(1 - p_2\, \mathrm{z}^{-1}) \\ &(1 - p_3\, \mathrm{z}^{-1}) \ldots (1 - p_i\, \mathrm{z}^{-1}) \\ &\begin{array}{ll} i = 4, \ldots, n + m + \delta - 1 & \forall\, n \geq 2 \\ i = 4, \ldots, n + m + \delta & \forall\, n = 1 \end{array} \end{aligned} \tag{35}$$

gives SDP-PID+ gains $\{k_{1,k},\ k_{2,k}, k_{3,k}, ..., k_{i,k}$ $(i = 4, ..., n + 1), k_{u_j,k} (j = 1, ..., m + \delta - 2)\}$ at pre-determined pole locations $\{p_1,\ p_2,\ p_3, ...,\ p_i$ $(i = 4, ..., n + m + \delta - 1\ \forall\, n \geq 2)\}$ in the complex z-plane. The control law can subsequently be extracted from Figure 3 in Equation (36).

$$\begin{aligned} u_k =& u_{k-1} + k_{1,k}\, e_k - k_{2,k}\, e_{k-1} + k_{3,k}\, e_{k-2} \\ &+ \sum_{i=4}^{n+1} k_{i,k}\, e_{k-(i-1)} \\ &- \sum_{j=1}^{m+\delta-2} k_{u_j,k} \left(u_{k-j} - u_{k-(j+1)}\right) \end{aligned} \tag{36}$$

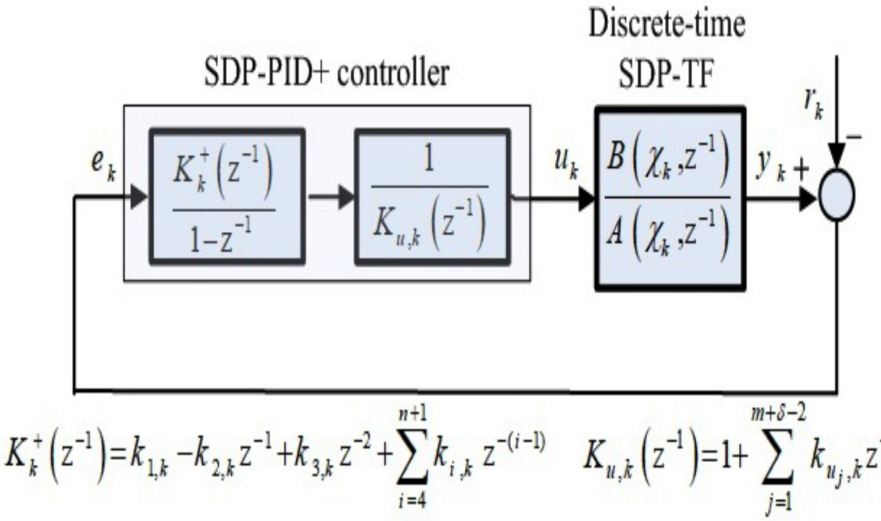

Figure 3. The regulator structure of the unity feedback closed loop SDP-PID+ control system.
Abbreviations: PID: Proportional integral derivative; SDP: State-dependent parameter; TF: Transfer function

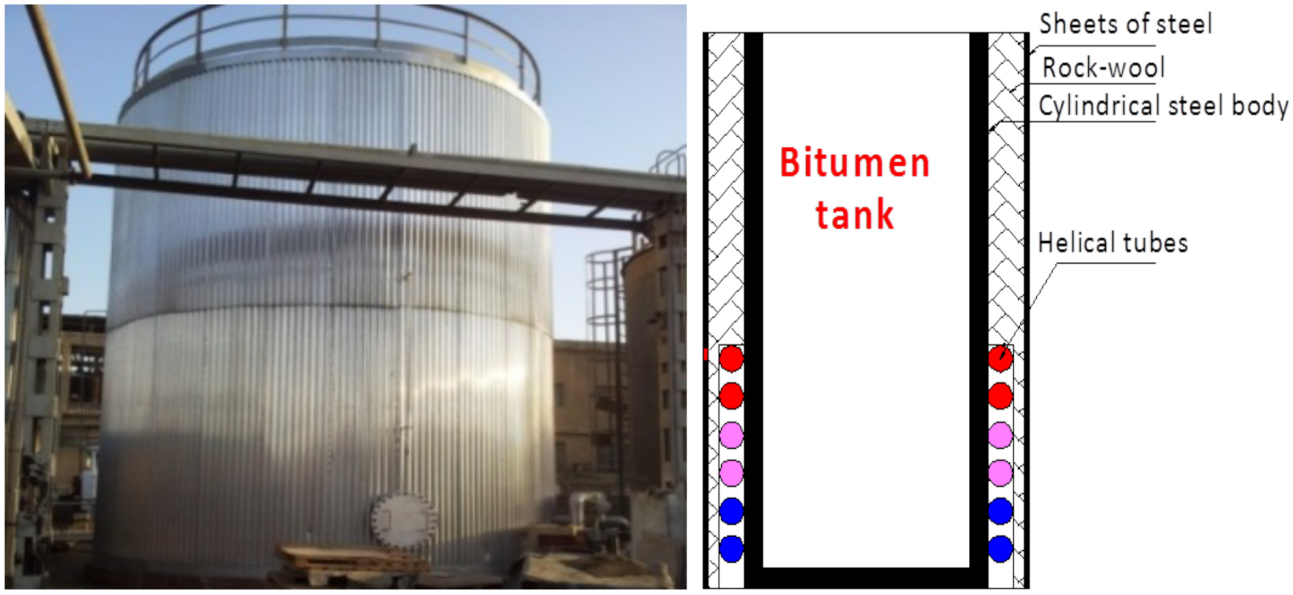

Figure 4. Bitumen tank at INSUMAT company, Tamouh, Giza, Egypt

Alternatively, the SVF/SDP-PID+ control action in Equation (24) can be directly used, where the parameters of the SVF/SDP-PID+ control vector, defined in Equation (25), are derived from Equation (34). It is worth noting that a systematic trial and error experiment is applied to analyze the closed-loop poles in the complex z-plane ($0 < p_i < 1$), aiming to determine appropriate gains that ensure a satisfactory tracking response.

4. Industrial bitumen tank

This tank, located at INSUMAT Company in Tamouh, Giza, Egypt, is used to heat raw liquid bitumen ($\sim 90°$C) before mixing to produce bitumen products. The properties of the final product depend significantly on the mixing temperature ($90 - 180°$C), which must remain within a $\pm 5\%$ range of the set value, as well as the quantity of additives used. To prevent overheating, the temperature must never reach the self-ignition point ($\sim 220°$C) of the vapor inside the tank.[10]

The bitumen tank is a closed steel reservoir enclosed by helical tubes filled with hot oil ($\sim 265°$C). Raw liquidized bitumen is fed into the tank via an inlet pipe at the top, and the heated bitumen is discharged to a blender through an outlet pipe near the base, as in Figure 4.

Rockwool blocks insulate the tank's exterior to minimize heat loss and reduce power consumption.

A motorized three-way valve and a PT100 temperature sensor are integrated into this thermal process and connected to a data acquisition unit (LabJack UE9) interfaced with a LabVIEW™ program. The valve's opening is normalized from 0 (fully closed) to 100 (fully open) to regulate the flow rate of the hot oil, functioning as an actuator. The PT100 provides temperature feedback for the control system. A LabVIEW™ module was developed to manage the hardware components (three-way valve and PT100 sensor) and apply the selected controller. Additional hardware/software interfacing details can be found in Hamed et al.[40]

4.1. State-dependent parameter model for bitumen tank

The bitumen tank's process exhibits a relatively slow dynamic response, prompting the selection of a sampling rate of one sample every four minutes, i.e., $\Delta t = 240$.[40] The analysis of the experimental data for Bitumen temperature produces an SDP-TF model with triad $\{1,\ 1,\ 3\}^{13}$, as shown below in Equation (37)

$$\begin{aligned} y_k &= -a_1(\chi_k)\, y_{k-1} + b_3\, u_{k-3} && \text{(i)} \\ a_1(\chi_k) &= 0.1 \times 10^{-5}\, y_{k-3}^2 - 0.00135\, y_{k-3} - 0.995 && \text{(ii)} \\ b_3 &= 0.063 \end{aligned} \tag{37}$$

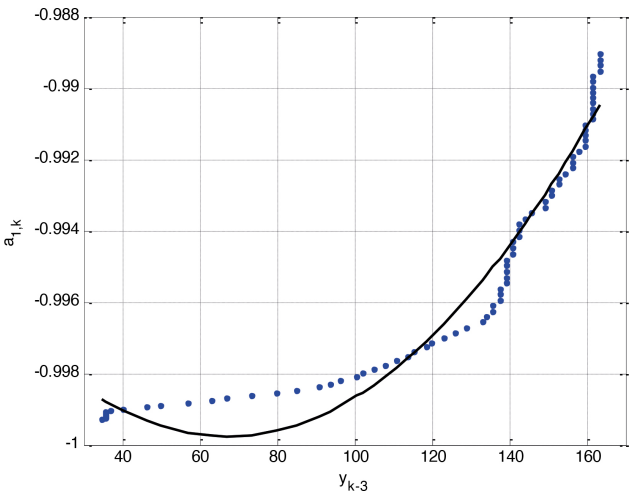

Figure 5. Estimated state-dependent parameter, $a_{1,k}$, versus its state variable y_{k-3}, i.e. $a_{1,k} = f\,(y_{k-3})$

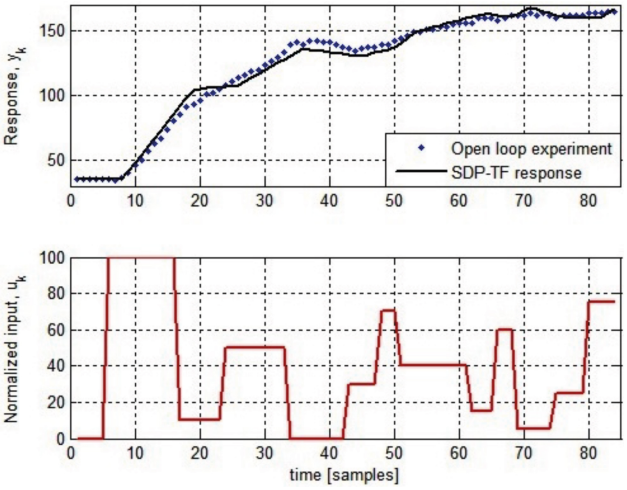

Figure 6. Open loop experiment and simulation results for the estimated SDP-TF model for bitumen temperature. Abbreviations: SDP, State-dependent parameter; TF, transfer function

where y_k represents the temperature of the bitumen, and u_k denotes the percentage of the three-way valve opening. The state-dependent output parameter $a_1(\chi_k)$, denoted as $a_{1,k}$, is time-variant, as shown in Figure 5, while the input parameter, denoted as b_3, is time-invariant. Figure 6 illustrates the simulation results for the estimated SDP-TF model in Equation (37).

4.2. Controller design and implementation for Bitumen temperature

Model in Equation (37) can be represented by using the operator z^{-1} as follows in Equation (38).

$$y_k = \frac{b_3\, \mathrm{z}^{-3}}{1 + a_1\,(\chi_{k+1})\ \mathrm{z}^{-1}}\, u_k \tag{38}$$

Using Equation (38) and Table 1, the nonlinear NMSS/SDP-PID+ form in Equation (7) can be constructed. As a result, the time-variant transition matrix $\mathbf{F}_k$ (5×5) at the k^{th} sample, and the time-invariant input vector $\mathbf{g}$ (5×1) and observation vector $\mathbf{h}$ (1×5) are defined using Equation (22) as follows in Equation (39).

$$\mathbf{F}_k = \begin{bmatrix} 1 & -a_1(y_{k-3}) & 0 & 0 & -b_3 \\ 0 & -a_1(y_{k-3}) & 0 & 0 & -b_3 \\ 0 & \dfrac{-a_1(y_{k-3}) - 1}{2} & \dfrac{1}{2} & 0 & \dfrac{-b_3}{2} \\ 0 & 0 & 0 & 0 & 0 \\ 0 & 0 & 0 & 1 & 0 \end{bmatrix},$$

$$\mathbf{g} = \begin{bmatrix} 0 \\ 0 \\ 0 \\ 1 \\ 0 \end{bmatrix}, \quad \mathbf{h} = \begin{bmatrix} 0 & 1 & 0 & 0 & 0 \end{bmatrix} \tag{39}$$

Here, the state vector, $\mathbf{x}_k$, for the bitumen system is defined as $\mathbf{x}_k = \begin{bmatrix} z_k & e_k & \Delta e_k & u_{k-1} & u_{k-2} \end{bmatrix}^T$. In this industrial example, SDP-PID+/LQ control was applied by freezing the parameters of $\{\mathbf{F}'_k,\ \mathbf{g}\}$ at ambient temperature, i.e. $y_{k-3} = 30^{\text{o}}$. Simulation trials showed that the weights $R = 1$ and $\mathbf{Q} = \text{diag}\{5\,1\,20000\,1\,1\}$ were appropriate for obtaining the time-invariant $\mathbf{P}$ matrix. Equation (30) was then used to calculate the SDP-PID+ gain vector, $\mathbf{k}_k^+$. Finally, the control law in Equation (24) was implemented for real-time bitumen temperature control, as depicted in Figure 7. This figure illustrates the practical implementation and simulation results of the SDP-TF model in Equation (38). It is worth noting that satisfactory rejection of the disturbances is shown when controlling the temperature of the bitumen.[13]

The nonlinear SDP-PID+/LQ control achieved suitable closed-loop performance, maintaining the response within the ±5% permissible range without overshooting. Negligible differences were observed between the practical and the SDP-TF model responses in Equation (38). This demonstration marks the first successful onsite application of SDP-PID+ control in an industrial bitumen system, providing robust temperature tracking and control performance.

5. Industrial reeling/packing machine

The industrial reeling/packing machine used in the bitumen membrane sheet production line at INSUMAT company, Sadat City, Egypt, incorporates nonlinear SDP-PID+ control methodology integrated into FPGAs. This control system manages the pulling motor that regulates the velocity of the floating drum. Its primary function is to maintain the bitumen sheet within the accumulator at an acceptable range (15–85%) by adjusting the motor's reference speed (Figure 8). The SDP/PID+ control system dynamically counteracts disturbances detected through a feedback encoder mounted on the floating drum. The FPGA-based control strategy uses the LabVIEW-FPGA module to enable simultaneous control operations. Detailed hardware and software interfacing is provided in Shaban *et al.*[15]

The system's primary objective is to prevent productivity losses caused by excessive infoldings of bitumen sheets around the reeling drum or interruptions due to emergency shutdowns. This would reduce reliance on operator skills and decrease workload, enhancing productivity and minimizing production costs.

5.1. State-dependent parameter model for reeling/packing machine

A SIEMENS's AC three-phase servo motor drives the reeling drum (7 kW/2000 rpm) through an analog input signal of 0-10 VDC. The encoder AUTONICS (2048 PPR/5-24 VDC) is installed on the floating drum to monitor its speed from 0 to 1500 rpm, as shown in Figure 9.

Open-loop experiments identified an optimal sampling rate, $\Delta t = 0.5$ sec, balancing accurate response measurement without redundant encoder reads. The experiments yielded an SDP-TF model with a triad $\{1,\ 1,\ 3\}$ as follows in Equation (40),

$$\begin{aligned} y_k &= -a_1(\chi_k)\, y_{k-1} + b_3(\chi_k)\, u_{k-3} \quad \text{(i)} \\ a_1(\chi_k) &= -0.0564\, u_{k-2} + 0.2836 \quad \text{(ii)} \\ b_3(\chi_k) &= -0.0675\, y_{k-1} + 192.0957 \end{aligned} \tag{40}$$

where y_k represents the floating drum's speed (rpm) and u_k is the voltage input to the AC three-phase servo motor of 0 to 10 VDC. The SDPs $a_1(\chi_k)$ and $b_3(\chi_k)$, denoted as $a_{1,k}$ and $b_{3,k}$ respectively, are time-variant and depicted in Figure 10. The model fit of the estimated SDP-TF in Equation (40) to experimental data achieved a satisfactory coefficient of determination, $R_T^2 = 0.95$, as illustrated in Figure 11.

5.2. Controller design and implementation for reeling/packing machine

By merging and rearranging Equation (40), the updated SDP-TF model is expressed as follows in Equation (41).

$$\begin{aligned} y_k = &-\left(0.0675\, u_{k-3} - 0.0564\, u_{k-2} + 0.2836\right) y_{k-1} \\ &+ 192.0957 u_{k-3} \end{aligned} \tag{41}$$

The SDPs may be further refined as Equation (42).

$$\begin{aligned} a_1(\chi_k) &= 0.0675\, u_{k-3} - 0.0564\, u_{k-2} + 0.2836 \\ b_3 &= 192.0957 \end{aligned} \tag{42}$$

The SDP-TF model in Equation (41) may be reformulated using the operator, z^{-1}, as Equation (43).

$$y_k = \frac{b_3\, \text{z}^{-3}}{1 + a_1\left(\chi_{k+1}\right) \text{z}^{-1}}\, u_k \tag{43}$$

Here, the output parameter $a_1\left(\chi_k\right)$, defined in Equation (42), is state-dependent on the lagged input $\chi_k = f\left(u_{k-3},\ u_{k-2}\right)$, while the input parameter b_3, is time-invariant.

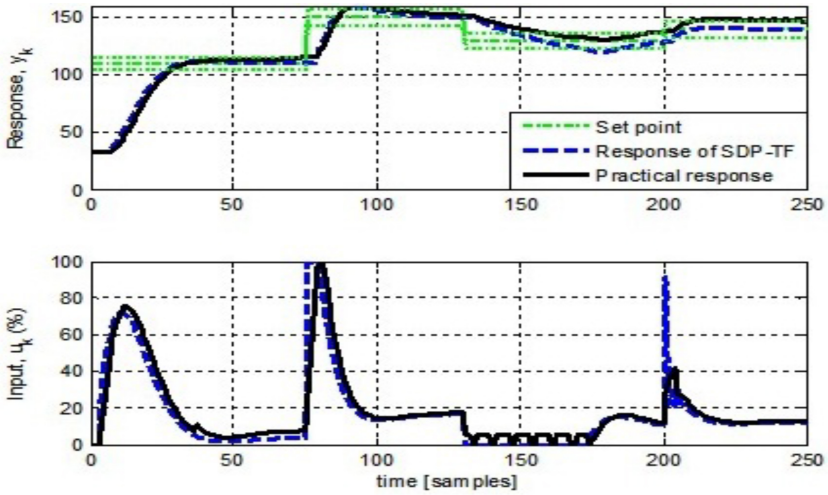

Figure 7. Onsite implementation of the SDP-PID+/LQ control for the bitumen tank, with the command input shown alongside its ±5% tolerance. Abbreviations: LQ, linear quadratic; PID+, proportional integral derivative plus; SDP, state-dependent parameter; TF, transfer function

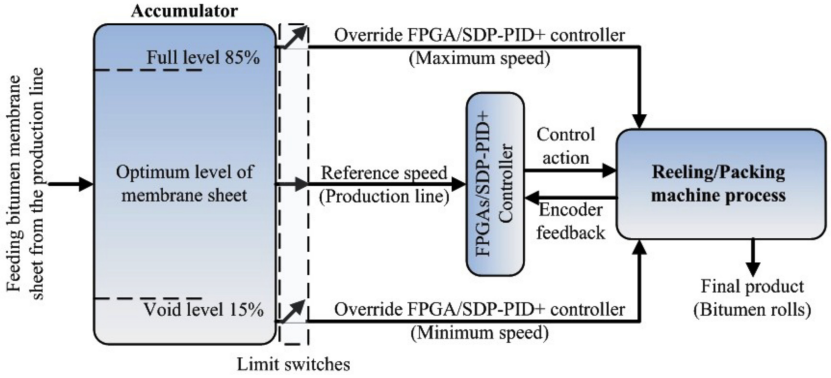

Figure 8. The control process of the reeling/packing machine for Bitumen membrane sheets employs the SDP-PID+ methodology, integrated in FPGAs, at INSUMAT company, Sadat City, Egypt. Abbreviations: FPGA, Field programmable gate array; PID+, Proportional integral derivative plus; SDP, State-dependent parameter.

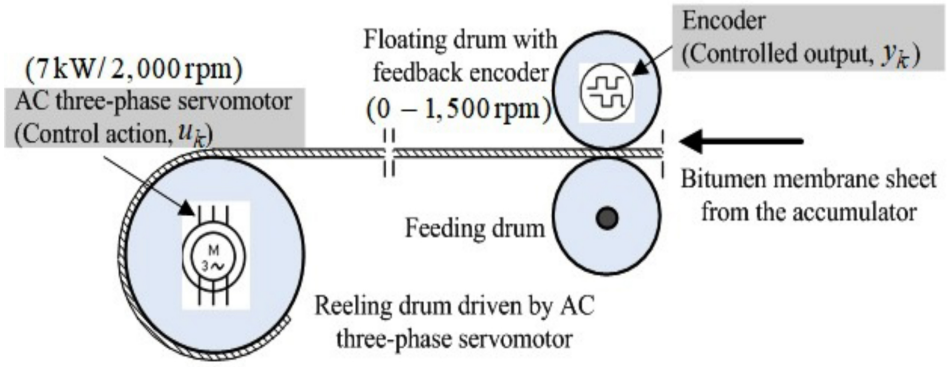

Figure 9. Schematic of the reeling/packing process for bitumen membrane sheets at INSUMAT company, Sadat City, Egypt. Abbreviation: AC, alternating current.

Using the model in Equation (43) and Table 1, the NMSS framework for nonlinear SDP-PID+ control is constructed, similar to the structure in Equation (39). The time-variant transition matrix $\mathbf{F}_k$, time-invariant input vector $\mathbf{g}$, and observation vector $\mathbf{h}$ remain consistent with the state vector $\mathbf{x}_k = \begin{bmatrix} z_k & e_k & \Delta e_k & u_{k-1} & u_{k-2} \end{bmatrix}^T$.

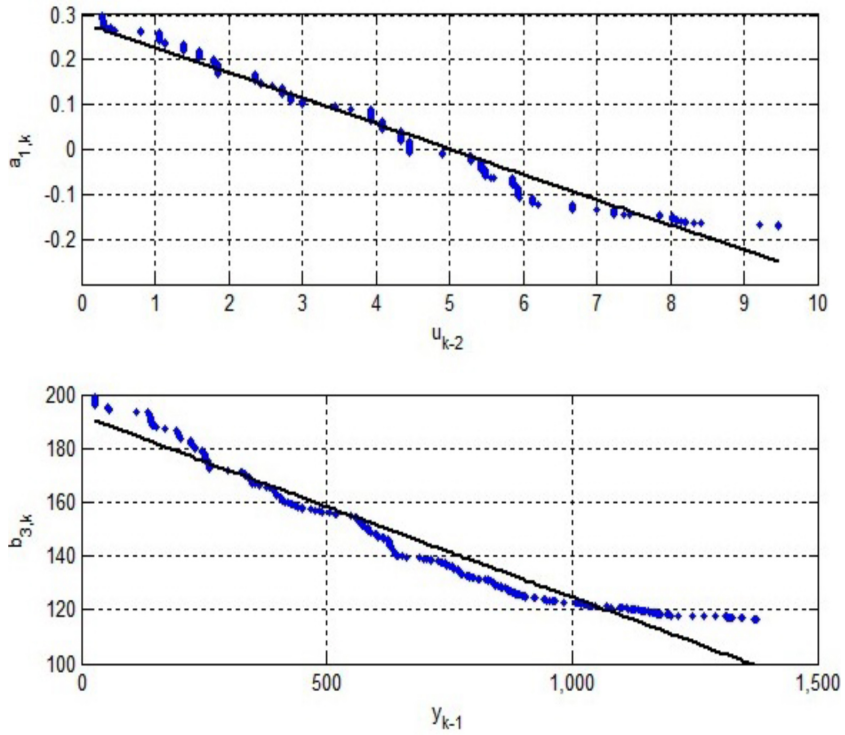

Figure 10. SDPs $a_1\,(u_{k-2})$ and $b_3\,(y_{k-1})$ of the SDP-TF model in Equation (40) versus their state variables. Abbreviations: SDP, State-dependent parameter; TF, transfer function.

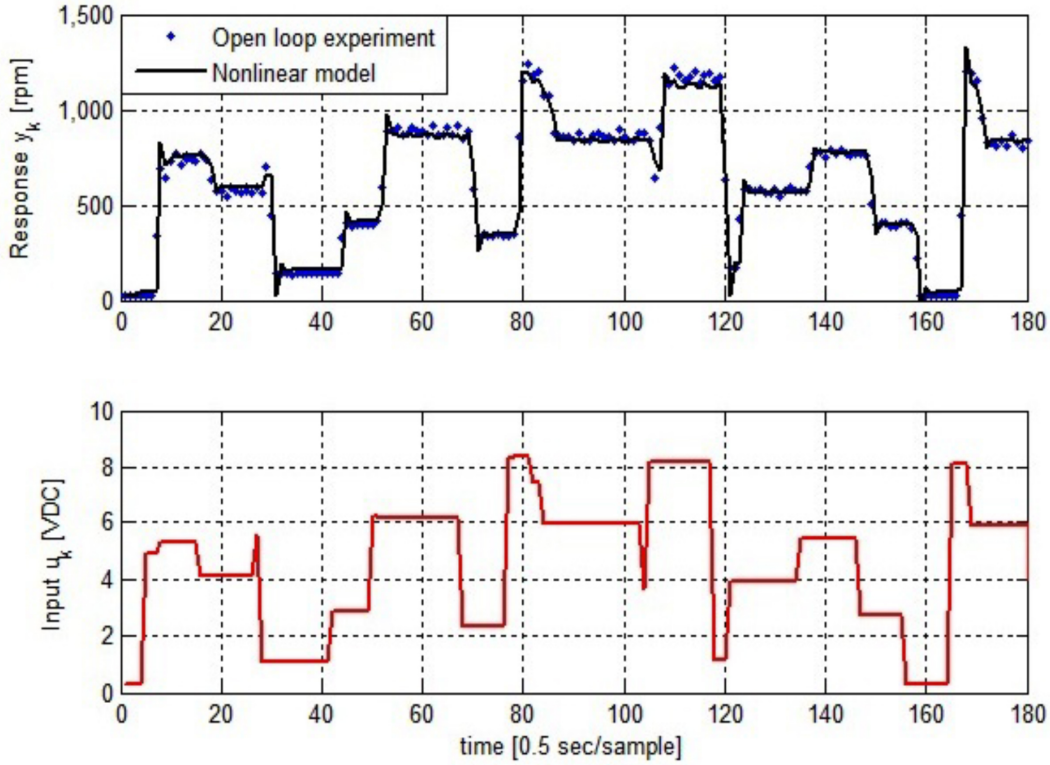

Figure 11. Open-loop experiment for the reeling/packing process with the simulation fit of the SDP-TF model in Equation (40). Abbreviations: SDP, State-dependent parameter; TF, transfer function; VDC, Volts direct current.

The time-invariant $\mathbf{P}$ matrix can be obtained by freezing $\mathbf{F}_k$ at a specific operating point $u_{k-2} = u_{k-3} = 0$. The weights $R = 1$ and $\mathbf{Q} = \text{diag}\ \{1\,1\,1\,1\,1\}$ were selected to obtain the time-invariant $\mathbf{P}$ matrix using algebraic Riccatti equation as defined in Equation (29). The time-variant SDP-PID+ gain vector, $\mathbf{k}_k^+$ is then computed using Equation (30). The control law in Equation (24) is employed to control the drum's reeling/packing machine speed, as shown in Figure 12.

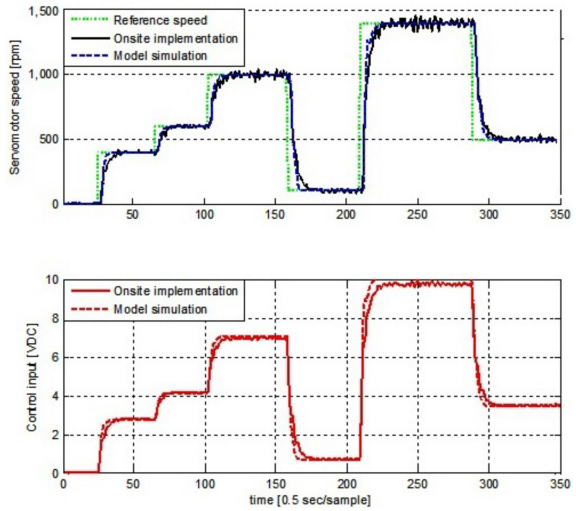

Figure 12. Onsite application of FPGAs/SDP-PID+ control for the industrial reeling/packing machine. Abbreviations: FPGA: Field programmable gate array; PID+: Proportional integral derivative plus; SDP: State-dependent parameter; VDC: Volts direct current.

The onsite implementation demonstrates that the FPGAs/SDP-PID+ control ensures acceptable performance with significant noise suppression and negligible differences between practical and SDP-TF model in Equation (40) responses. No overshoot or severe oscillations were observed, confirming robust control for the reeling/packing process. It is worth noting that the feasibility of FPGA implementation for real-scale industrial systems, including processing power and memory constraints, is detailed in Shaban et al.,[15] where all relevant hardware features are analyzed.

6. Conclusion

This paper presented the expansion and practical implementation of SDP-PID+ control systems across two distinct demonstrators: an industrial bitumen tank system and an industrial reeling/packing machine used in the bitumen membrane sheet production line. This enhancement enables efficient and intuitive control of these systems, which are characterized by discrete-time TFs of any order and sampling time delays.

The selected demonstrators represent the first industrial implementations of the SDP-PID+ control methodology, showcasing its applicability across systems with varying response times, 240 and 0.5 s, respectively, providing a comprehensive evaluation of their performance.

In all cases, the systems were modeled using the quasi-linear SDP model structure, where parameters depend on other system variables. This model structure allowed for designing an SDP-PID+ control law to leverage linear system design strategies such as suboptimal LQ optimization or pole placement. Importantly, the control gains were made state-dependent, enhancing adaptability and performance. Notably, the time-invariant numerator parameter in models in Equations (38) and (43) satisfies the two controllability conditions discussed in Section (3.2).

The proposed control strategy markedly improved temperature regulation for the industrial bitumen tank system, maintaining it consistently within the $\pm 5\%$ permissible range while avoiding overshoot. This enhanced performance minimized the risk of vapor self-ignition inside the tank, ensuring greater operational safety and improved quality of the bitumen mixture.

Finally, implementing the FPGAs/SDP-PID+ control for the industrial reeling/packing machine demonstrated robust closed-loop performance. The system exhibited no overshoot, no severe oscillations, and effective noise reduction, attributed to the advanced real-time processing capabilities of FPGA technology.

The results from these diverse demonstrators confirm the effectiveness of the extended SDP-PID+ control in optimizing design time, enhancing practicality, and improving adaptability and robustness. Its ability to accommodate systems with varying dynamics while ensuring superior performance and operational reliability highlights its potential as a versatile control strategy for industrial applications. Future work may extend this approach to more complex multivariable systems and optimize its implementation for improved computational efficiency.

Acknowledgments

The author gratefully acknowledges the support of the Deanship of Graduate Studies and Scientific Research, Jazan University, Saudi Arabia.

Funding

None.

Conflict of interest

The author has no relevant financial or non-financial interests to disclose.

Author contributions

This is a single-authored article.

Availability of data

Data will be made available upon request to corresponding author.

References

1. Borase RP, Maghade DK, Sondkar SY, Pawar SN. A review of PID control, tuning methods, and applications. *Int J Dyn Control.* 2021;9:818–827. http://dx.doi.org/10.1007/s40435-020-00665-4.
2. Bennett S. Development of the PID controller. *IEEE Control Syst Mag.* 1993;13(6):58–62. https://doi.org/10.1109/37.248006.
3. Liu L, Lv W, Liu J, et al. Performance of active-quenching SPAD array based on the tri-state gates of FPGA and packaged with bare chip stacking. *Sensors*, 2023;23(9):4314. https://doi.org/10.3390/s23094314
4. Vega P, Prada C, Aleixandre V. Self-tuning predictive PID controller. *IEE Proc D: Control Theory Appl.* 1991;138:303–312. http://dx.doi.org/10.1049/ip-d.1991.0041
5. Porter B, Jones AH. Genetic tuning of digital PID controllers. *Electron Lett.* 1992;28(9):843–844. IET Digital Library.
6. Åström KJ, Hägglund T, Hang CC, Ho WK, Automatic tuning and adaptation for PID controllers: a survey. *Control Eng Pract.* 1993;1(4):699–714. http://dx.doi.org/10.1016/0967-0661(93)91394-C.
7. Leva A. PID autotuning algorithm based on relay feedback. *IEEE Proc D Control Theory Appl.* 1993;140:328–338. http://dx.doi.org/10.1049/ip-d.1993.0044.
8. Khodadadi H, Ghadiri H. Self-tuning PID controller design using fuzzy logic for half-car active suspension system. *Int J Dyn Control.* 2018;6(1):224–232. http://dx.doi.org/10.1007/s40435-016-0291-5.
9. Loiseau J-J, Boudana M, Ladaci S. Fractional order PIDμ control design for a Class of cyber-physical systems with fractional order time-delay models. *Int J Cyber Phys Syst.* 2019;1(2):1–18. http://dx.doi.org/10.4018/IJCPS.2019070101.
10. Hamed AR, Shaban EM, Darwish RR, Abdel Ghany AM. Design and implementation of discrete PID control applied to Bitumen tank based on a new approach of pole placement technique. *J of Dyn Control.* 2017;5(3):604–613. https://doi.org/10.1007/s40435-015-0199-
11. Shaban EM, Sayed H, Abdelhamid A. A novel discrete PID+ controller applied to higher-order/time-delayed nonlinear systems with practical implementation. *J Dyn Control.* 2019;7(3):888–900. https://doi.org/10.1007/s40435-018-0472-5
12. Sayed H, Shaban EM, Abdelhamid A. State dependent parameter PID+ control applied to a nonlinear manipulator arm. In: *RAEMP 2019 International Conference on Recent Advances in Engineering Mathematics and Physics*, Dec 24–26. Springer, Cairo, Egypt; 2019. http://dx.doi.org/10.1007/978-3-030-39847-7$_1$
13. Hamed AR, Shaban EM, Abdelhaleem, Abdel Ghany AM. Industrial implementation of state dependent parameter PID+control for nonlinear time-delayed Bitumen tank system. *Iran J Sci Technol - Trans Electr.* 2022;46(11):743–751. https://doi.org/10.1007/s40998-022-00488-3
14. Bashiri AH. Empirical study of robust/developed PID control for nonlinear time-delayed dynamical system in discrete time domain. *Heliyon*, 2024;10(9). http://dx.doi.org/10.1016/j.heliyon.2024.e11935
15. Shaban EM, Hamed AR, Bassiuny AM, Abdelghany AM. On implementation of nonlinear PID+controller embedded on FPGA module for industrial system. *Int J Dyn Contr.* 2023;12(7):2331–2340. https://doi.org/10.1007/s40435-023-01338-8
16. Taylor CJ, Young PC, Chotai A. State-space control system design based on non-minimal state-variable feedback: further generalization and unification results. *Int J Control.* 2000;73:1329–1345. http://dx.doi.org/10.1080/00207170010004698.
17. Shaban EM, Hamed AR, Darwish RR, Abdel Ghany AM. New tuning approach of discrete PI/PID controller applied to Bitumen system based on non-minimal state-space formulation. In: *ICCTA 2015, IEEE 25th International Conference*, Oct 24–26, Alexandria, Egypt. IEEE Xplore Digital Library; 2015:52–57.
18. Shaban EM, Ako S, Taylor CJ, Seward DW. Development of an automated verticality alignment system for a vibro-lance. *Autom Constr.* 2008;17(5):645–655. http://dx.doi.org/10.1016/j.autcon.2007.08.001
19. Taylor CJ, Shaban EM, Stables MA, Ako S. Proportional-integral-plus control applications of state-dependent parameter models. Part I: *J Syst Control Eng.* 2007;221(7):1019–1031. https://doi.org/10.1243/09596518JSCE366
20. Stables MA, James CJ. Non-linear Control of Ventilation Rate using State-dependent Parameter Models. *Biosyst Eng.* 2006;95(1):7–18, ISSN 1537–5110. https://doi.org/10.1016/j.biosystemseng.2006.05.015
21. Taylor CJ, Robertson D. State-dependent control of a hydraulically actuated nuclear decommissioning robot. *Control Eng Pract.*

2013;21(12):1716–1725.
http://dx.doi.org/10.1016/j.conengprac.2013.06.003
22. Deepa SN, Sugumaran G. Design of PID controller for higher-order continuous systems using MPSO-based model formulation technique. *Int J Electr Electron Eng.* 2011;5(4):289–295.
http://dx.doi.org/10.5281/zenodo.1056472
23. Young PC. Stochastic, dynamic modelling and signal processing: Time variable and state dependent parameter estimation. In: Fitzgerald WJ, ed. *Nonlinear and Nonstationary Signal Processing*. Cambridge University Press; 2000.
http://dx.doi.org/10.1016/B978-0-7506-7359-4.50015-9
24. Shaban EM, James CJ, Chotai A. State dependent parameter, proportional-Integral-Plus (SDP-PIP) control of a Nonlinear Robot Digger Arm. In: *UKACC Control 2004, University of Bath*, Bath, UK, ID–059. 2004;
http://dx.doi.org/10.1016/j.ifacol.2005.10.053
25. Dixon R, Taylor CJ, Shaban EM. Comparison of classical and modern control applied to an excavator-arm. International Federation of Automatic Control 16th Triennial World Congress (IFAC-05), Prague, Czech Republic. 2005;38(1):589–594.
http://dx.doi.org/10.3182/20050703-6-CZ-1902.01368
26. Shaban EM, Zied K, Taylor CJ, Seward DW. Nonlinear control system design for construction robots: estimation, partial linearization by feedback and state-dependent-parameter control, 22nd International Symposium on Automation and Robotics in Construction (ISARC-05), Ferrara, Italy; 2005.
https://doi.org/10.22260/ISARC2005/0041.
27. Shaban EM, Nada AA. On linearization of nonlinear dynamic systems described by state-dependent-Parameter (SDP) Discrete-Time Model. In: *5th European Conference on Computational Mechanics (ECCM V)*, Barcelona, Spain. CIMNE - ECCM V Proceedings; 2014: 538–547.
28. Young PC. Recursive Estimation and Time Series Analysis. Springer-Verlag; 1984.
http://dx.doi.org/10.1007/978-3-642-21981-8
29. Young PC. Simplified Refined Instrumental Variable (SRIV) estimation and True Digital Control (TDC): A tutorial introduction. 1st European Control Conference: Grenoble, France.1991;1295–1306.
30. Janot A, Young PC, Gautier M. Identification and control of electro-mechanical systems using state dependent parameter estimation. *Int J Control.* 2017;90(4):643–660.
http://dx.doi.org/10.1080/00207179.2016.1209565
31. Taylor CJ, Pedregal DJ, Young PC, Tych W. Environmental time series analysis and forecasting with the Captain Toolbox. *Environ Model Softw.* 2007;22:797–814.
http://dx.doi.org/10.1016/j.envsoft.2006.06.002
32. Young PC, Taylor CJ, Tych W, Pedregal DJ. The Captain Toolbox. Center for Research on Environmental Systems and Statistics, Lancaster University:UK. 2007.
http://www.es.lancs.ac.uk/cres/captain
33. He J-B, Wang Q-G, Lee T-H. PI/PID controller tuning via LQR approach. *Chem Eng Sci.* 2000;55(13):2429–2439.
http://dx.doi.org/10.1016/S0009-2509(99)00512-6
34. Das S, Pan I, Halder K, Das S, Gupta A. Optimum weight selection-based LQR formulation for the design of fractional-order PID controllers to handle a class of fractional-order systems. In: *International Conference on Computer Communication and Informatics (ICCCI)*, Jan 4, IEEE; 2013: pp. 1–6;
http://dx.doi.org/10.1109/ICCCI.2013.6466137
35. Young PC, Behzadi MA, Wang CL, Chotai A. Direct digital and adaptive control by input-output, state-variable feedback pole assignment. *Int J Control.* 1987;46:1867–1881.
http://dx.doi.org/10.1080/00207178708934274
36. McCabe AP, Young PC, Chotai A, Taylor CJ. Proportional-Integral-Plus (PIP) control of nonlinear systems.*Syst Sci.* 2000;26:25–46.
http://dx.doi.org/10.1002/sys.10004
37. Åström KJ, Wittenmark B. Computer Controlled Systems: Theory and Design. *Prentice-Hall Information and System Sciences Series*. 1984.
38. Shaban EM. Deadbeat response of nonlinear systems described by discrete-time state dependent parameter using exact linearization by local coordinate transformation. *J Am Sci.* 2012;8(10):355–366.
http://dx.doi.org/10.7537/j.issn.1545-1003.2012.10.053
39. Shaban EM, Taylor CJ. Proportional-Integral-Plus control of a class of nonlinear systems using exact and partial linearization by feedback. *ICGST Int J Autom Control Syst Eng.* 2006;6:55–70.
http://dx.doi.org/10.1109/ICCCI.2013.6466137
40. Hamed AR, Darwish RR, Shaban EM, Abdel Ghany AM. Hardware synthesis and dynamic modeling of Bitumen tank. *J Am Sci.* 2014;10(12):183–189.
http://dx.doi.org/10.7537/j.issn.1545-1003.2014.12.021

E. M. Shaban *was born on July 15, 1967, in Cairo, Egypt. He earned his Ph.D. in True Digital Control (TDC) and System Dynamics from Lancaster University, Lancaster, UK, in 2006. Currently, Dr. Shaban is an Associate Professor in the Mechanical Engineering Technology Department at the College of Applied Industrial Technology, Jazan University (KSA), while on leave from the Faculty of Engineering (Mattaria), Helwan University. His research focuses on the control of highly nonlinear systems, with an emphasis on improving controller robustness.*

 https://orcid.org/0000-0002-5678-6183

An International Journal of Optimization and Control: Theories & Applications
(https://accscience.com/journal/ijocta)